

A comparison of annealing process and nucleating agent (zinc phenylphosphonate) on the crystallization, viscoelasticity, and creep behavior of compression-molded poly(lactic acid) blends



Teng-Chun Yang^a, Ke-Chang Hung^a, Tung-Lin Wu^a, Tzong-Ming Wu^b, Jyh-Horng Wu^{a,*}

^a Department of Forestry, National Chung Hsing University, Taichung 402, Taiwan

^b Department of Materials Science and Engineering, National Chung Hsing University, Taichung 402, Taiwan

ARTICLE INFO

Article history:

Received 17 June 2015

Received in revised form

10 September 2015

Accepted 15 September 2015

Available online 18 September 2015

Keywords:

Poly(lactic acid)

Annealing

Zinc phenylphosphonate

Viscoelasticity

Time–temperature superposition principle

Creep behavior

ABSTRACT

In this study, the thermal crystallization, viscoelastic property, and creep behavior of poly(lactide acid)/zinc phenylphosphonate (PLA/PPZn) blends were compared with those of annealed PLA. The results revealed that PPZn exhibited an excellent nucleating effect for the crystallization of PLA. The isothermal crystallization half-time ($t_{1/2}$) of amorphous PLA (PLA_{am}) at 130 °C was 28.1 min, whereas all the $t_{1/2}$ values of PLA/PPZn blends were less than 1 min. In addition, the blends showed better thermal resistance than the annealed PLA. The storage modulus (E') of all the PLA/PPZn blends was higher than that of the annealed PLA at temperatures higher than the T_g of PLA. However, the modulus of rupture (MOR) of PLA/PPZn blends decreased with increasing PPZn concentration in the PLA matrix, whereas there was no noticeable difference for all the annealed PLA. Regarding the creep behavior, the predicted modulus reduction of PLA_{am} was 42.9% at 60 years by time–temperature superposition principle (TTSP) method. In contrast, the reductions in modulus levels of all the PLA/PPZn blends and the annealed PLA were still less than 33% over the 60-year period.

© 2015 Elsevier Ltd. All rights reserved.

1. Introduction

Poly(lactic acid) (PLA) is renewable, biomass-derived, biocompatible, and nontoxic to the environment and human body; thus, it has attracted considerable attention for its broad application in the biomedical, agricultural, and packaging industries. Additionally, PLA has raised considerable interest as a potential substitution for petroleum-based polymers because of its favorable biodegradability, versatile fabrication, and good mechanical properties [1]. However, one of the general drawbacks of PLA-based materials is its low glass transition temperature (ca. 56 °C), which severely limits the application of PLA. It is well known that most properties of PLA are mainly dependent on the crystalline morphology, spherulite size, and crystallinity [2–4]. The crystalline form is required to increase the thermal resistance of PLA. Therefore, annealing treatment is commonly used to develop the crystal region of amorphous PLA (PLA_{am}), which results in the formation of the crystallized polymer. According to previous studies [5–8], the minimum

crystallization half-time or the maximum crystallization rate was reached in the range of 105–110 °C.

The other drawback of PLA-based materials is the slow crystallization rate that causes almost no crystallization under a high cooling rate during the practical molding process [9]. The heterogeneous nucleation, in which additional impurities are present in the polymer matrix as heterogeneous nuclei, reduces the free energy needed for the formation of a critical nucleus to increase the crystallization rate. The overall nucleation and crystallization rates of PLA in heterogeneous conditions are relatively higher than in homogenous conditions. In general, nucleating agents that can be added to the PLA matrix have been developed, and they have been shown to be an effective approach to reduce the nucleation induction time and increase the number of primary nucleation sites. Changes in the properties of nucleating agents that are added to polymers could be attributed to the quantity of spherulite, the filler loading, and the interfacial adhesion between the filler and the polymer matrix.

Recently, several researchers have attempted to reduce the induction time of nucleation and increase the nucleation density of PLA composites with inorganic fillers [10–16]. Pan et al. [17] reported that a few metal phosphonate filler-loaded PLA composites

* Corresponding author.

E-mail address: eric@nchu.edu.tw (J.-H. Wu).

can accelerate the crystallization rate and improve the mechanical properties. Zinc phenylphosphonate (PPZn), one of the most famous nucleation agents, has a layered structure similar montmorillonite clay [18], and it can increase significantly the crystallization rate of PLA [17,19]. Although several studies have focused on the effects of homogeneous or heterogeneous nucleations on the crystallization rate and thermal and mechanical properties, a limited number of studies have investigated the difference between these two crystallization processes on various properties in a PLA matrix. In addition, polymer composites exhibit a time-dependent degradation in modulus and strength as a consequence of the viscoelasticity of the polymer matrix [20]. In most practical applications, creep behavior, which is a time-dependent response, is of considerable significance because isothermal compliance of the polymeric material depends not only on stress but also on time. Therefore, the creep behavior is a critical issue for many engineering fields, such as aerospace and biomedical engineering. Several studies have been conducted on the creep behavior of polymer matrix composites. For example, the flexure creep properties of E-glass reinforced polymers were studied by Abdel-Magid et al. [21]. Wang et al. [22] reported the creep behavior of basalt fiber-reinforced polymer tendons. For polymeric matrix with natural fibers, Doh et al. [23] studied the creep behavior of liquefied wood–polymer composites based on polypropylene (PP), low-density polyethylene (LDPE), and high-density polyethylene (HDPE). For PLA composites, Suryanegara et al. [24] studied the creep deformation of microfibrillated cellulose-reinforced partially crystallized PLA composites. The creep behavior of PLA with lignin-based flax composites subjected to tensile loading was reported by Rozite et al. [25]. Kontou et al. [26] implemented nonlinear viscoelastic/viscoplastic response under monotonic loading and creep recovery tests of PLA composite with flax fibers. However, creep research that considers the difference between homogeneous and heterogeneous nucleations for PLA-based materials has not been conducted. To the best of our knowledge, there has not been any prior research on the comparison of nucleating agents and annealing on the thermal properties, mechanical properties, and creep behavior of compression-molded PLA blends. In this study, the thermal crystallization, viscoelastic property, and creep behavior of PLA/PPZn blends compared with the annealed PLA were investigated.

2. Experimental

2.1. Materials and preparation of blends

Semicrystalline grade comprised of approximately 2% D-LA oligomer PLA was purchased from Natureworks (PLA 4032D, Blair, NB). PPZn was purchased from Nissan Chemical Industries, Ltd. (Tokyo, Japan). PLA with various PPZn concentrations was compounded at 150 °C by a twin-screw extruder at a speed of 60 rpm. The mixtures were extruded and pelleted, then the plate samples with a thickness of 4.0 mm were hot-pressed at 180 °C after melting for 3 min, followed by quenching to room temperature. The PLA/PPZn blends are denoted as N_x , where x is the weight percent of PPZn in the blends. The annealed PLA are denoted as A_y , where y is the duration (min) of annealing at 110 °C.

2.2. Differential scanning calorimetry (DSC)

The crystallization behavior was measured by DSC 8500 (Perkin–Elmer, UK) with an intracooler II cooling accessory. The samples were weighed and sealed in an alumina pan. To measure the melt crystallization temperature, the samples were cooled from the melt state to room temperature at 10 °C/min after melting at 200 °C

for 5 min (non-isothermal crystallization). The degree of crystallinity (X_{mc}) was obtained as a function of the PPZn concentration using the following equation (1):

$$X_{mc}(\%) = \frac{\Delta H_m}{\Delta H_m^0 \times W_p} \times 100 \quad (1)$$

where ΔH_m is the experimental heat of fusion determined from the DSC measurement, ΔH_m^0 is the assumed heat of fusion of the fully crystalline PLA (93 J/g) [27], and W_p is the weight percentage of PLA in the blends. In addition, to investigate the crystallization half-time from isothermal conditions, the samples were rapidly cooled at 100 °C/min from the melt state to the desired temperature.

2.3. X-ray diffraction (XRD)

X-ray diffractograms were recorded with a MAC science MXP18 instrument (Japan) using Ni-filtered $CuK\alpha_1$ radiation ($\lambda = 0.1542$ nm) at 40 kV and 30 mA. XRD patterns of samples were recorded in the 2θ ranges of 4–40° with a scan rate of 2°/min. The crystallinity index (CrI) of the samples was calculated by the following equation (2) according to the previous study [28]:

$$CrI(\%) = \frac{A_{cry}}{A_{cry} + A_{am}} \times 100 \quad (2)$$

where A_{cry} is the area of the PLA crystallographic form at $2\theta = 16.5^\circ$ (planes 110 and 200) and 18.9° (plane 203), and A_{am} is the area of diffraction of the amorphous region.

2.4. Gel permeation chromatography (GPC)

A gel permeation chromatography (GPC) equipped with a PU-2080 pump (Jasco, Japan), a RI-2031 refractive index detector (Jasco, Japan), and 10E3A/10E4A columns (Phenogel, USA) was used to measure the number average molecular weight (M_n) and the weight average molecular weight (M_w) of the PLA/PPZn specimens. Tetrahydrofuran (THF) was used as the isocratic mobile phase at a flow rate of 1 mL/min. A series of polystyrene calibration standards was used to calculate M_n and M_w . Before sample injection, the specimens were dissolved in THF and then filtered through a 0.2- μ m hydrophilic polypropylene (GHP) membrane to remove insoluble particles.

2.5. Dynamic mechanical analysis (DMA)

The dynamic mechanical properties were measured in a single-cantilever bending mode (DMA 2000, PerkinElmer, Buckinghamshire, UK) with a span of 20 mm at a frequency of 1 Hz and a heating rate of 2 °C/min from room temperature to 170 °C. The samples were thin rectangular strips with dimensions of $30 \times 10 \times 4$ mm³.

The creep compliance master curves and activation energy of the glass transition relaxation were also determined by DMA. Creep and creep recovery cycles were conducted at isotherms between 20 and 50 °C in intervals of 5 °C. A three-point bending mode with a span of 40 mm was used. For each isotherm, 10% of the average flexural strength was applied for 1 h, followed by a 1 h recovery period. According to the principle of time–temperature superposition, each curve was shifted by an appropriate shift factor, $\log a_T$. This shift factor can be related to temperature and activation energy using the following Arrhenius equation (3):

$$\log \alpha_T = \frac{E_a}{R} \left[\frac{1}{T} - \frac{1}{T_{\text{ref}}} \right] \times \log e \quad (3)$$

where α_T is the horizontal shift factor, E_a is the activation energy of the glass transition relaxation (J/mol), T_{ref} is the reference temperature (K), T is the test temperature (K), and R is the universal gas constant (8.314 J/K/mol) [29,30]. Furthermore, the E_a is calculated from the slope of the plot of $\ln(f)$ versus $1/T_g$ according to equation (4):

$$E_a = -R \left[\frac{d(\ln(f))}{d(1/T_g)} \right] \quad (4)$$

where f is frequency (Hz), and T_g is the glass transition temperature determined from the peak of the $\tan \delta$ curves [31]. This measurement was conducted in dual cantilever mode under isochronal conditions at frequencies of 4, 8, 12, 16, 20, 24, 28, and 32 Hz. The master curves were modeled with the Findley power law [32], which is presented in following equation (5):

$$S(t) = S_0 + at^b \quad (5)$$

where $S(t)$ is the time-dependent compliance, S_0 is the instantaneous elastic compliance, a and b are constant numbers, and t is the elapsed time.

2.6. Flexural test

The flexural properties of all samples were determined according to the ASTM D 790-07. The sample was cut to $80 \times 16 \times 4 \text{ mm}^3$, and conditioned at $20 \pm 2 \text{ }^\circ\text{C}$ and $65 \pm 5\%$ relative humidity for 1 week before testing. The modulus of rupture (MOR) and modulus of elasticity (MOE) were obtained by the three-point static bending test with a loading speed of 1.7 mm/min and with a span of 64 mm.

2.7. Static analysis

All the results are expressed as the mean \pm standard deviation (SD). The significance of the differences was calculated by Scheffe's test, and P values < 0.05 were considered significant.

3. Results and discussion

3.1. Nonisothermal and isothermal crystallization

The effect of PPZn concentration on the nonisothermal crystallization of PLA was measured by DSC. As shown in Fig. 1a and Table 1, the exothermic melt crystallization peak (T_{mc}) of PLA_{am} is not detected upon cooling at $10 \text{ }^\circ\text{C}/\text{min}$ because its crystallization rate is too slow to reach completion. In contrast, an exothermic cold crystallization peak (T_{cc}) ($114.2 \text{ }^\circ\text{C}$) is observed in the subsequent re-heating process (Fig. 1b). With 0.5 wt% PPZn, the crystallization of PLA/PPZn blend ($N_{0.5}$) is completed upon cooling, and its T_{mc} is $123.4 \text{ }^\circ\text{C}$. With increasing PPZn concentration, the T_{mc} becomes sharp and subsequently shifts to a higher temperature. Upon the addition of 5 wt% PPZn, the T_{mc} of the PLA/PPZn blend (N_5) increased to $127.9 \text{ }^\circ\text{C}$. These results indicate that not only does the crystallization rate of PLA becomes faster but also the T_{mc} value increases when the PPZn loading in the PLA matrix is increased. Generally, the crystals formed at higher T_{mc} have larger lamellar thickness; thus, they possess a higher degree of crystallinity (X_{mc}) as shown in Table 1.

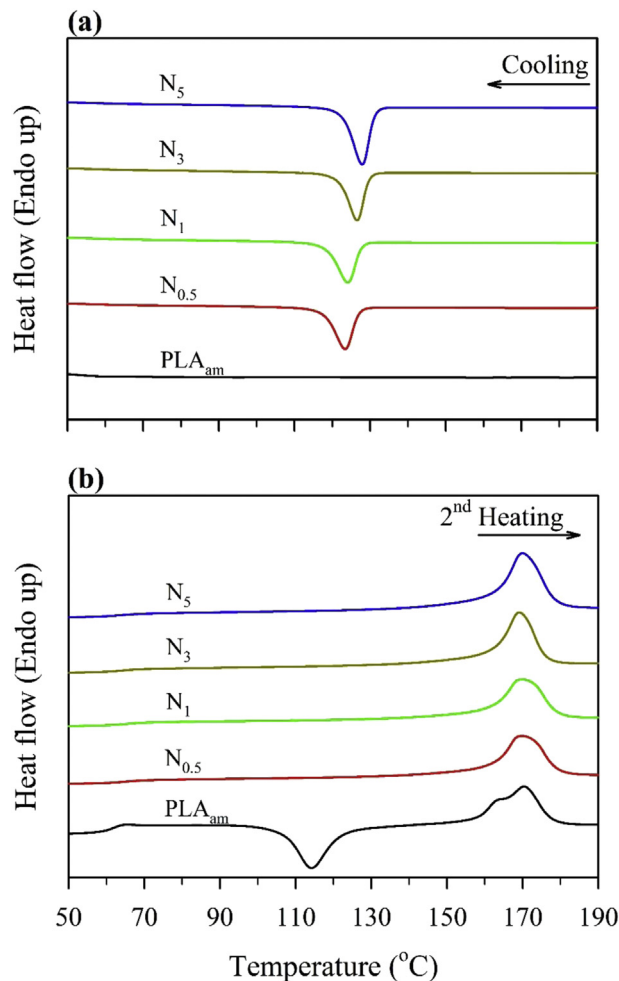


Fig. 1. DSC curves recorded during the cooling period at $10 \text{ }^\circ\text{C}/\text{min}$ (a) and the subsequent heating processes at $20 \text{ }^\circ\text{C}/\text{min}$ (b) for PLA/PPZn blends with different PPZn concentrations.

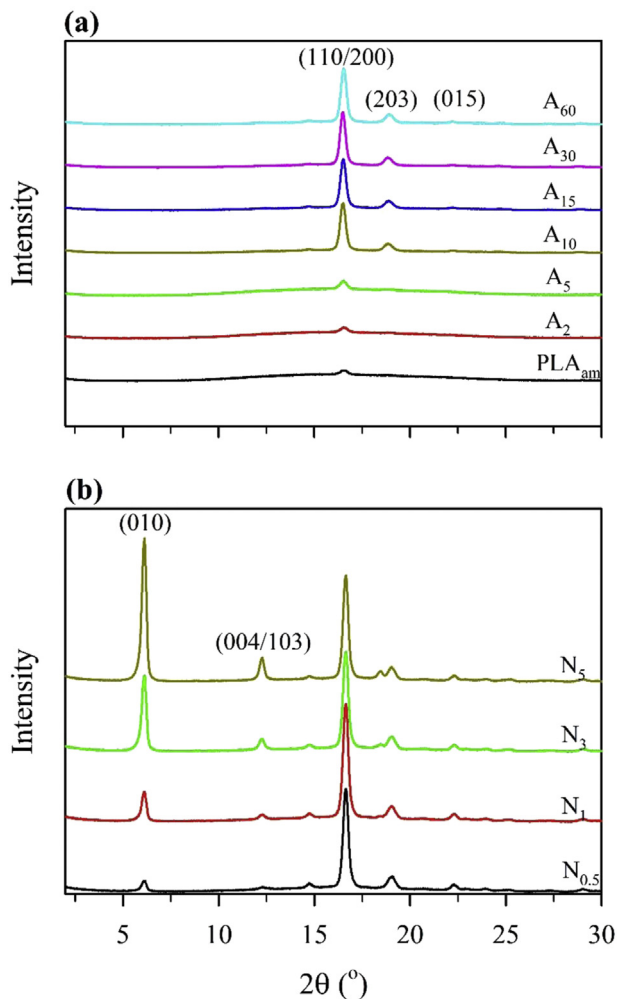
Furthermore, the addition of PPZn into PLA was also investigated in terms of crystallization half-time ($t_{1/2}$) which is defined as the time when half of the final crystallinity is reached under isothermal conditions. The results from nonisothermal crystallization indicated that the onset of the crystallization temperatures was approximately $130 \text{ }^\circ\text{C}$ upon cooling (Fig. 1a). Therefore, the fixation temperature was established at $130 \text{ }^\circ\text{C}$ to conduct the isothermal crystallization. As shown in Table 1, the $t_{1/2}$ value of PLA_{am} crystallizing at $130 \text{ }^\circ\text{C}$ is 28.1 min. However, all the $t_{1/2}$ values of PPZn-loaded PLA samples at $130 \text{ }^\circ\text{C}$ are less than 1 min. This result implies that the addition of PPZn into PLA matrix is applicable for industrial mold processing due to its rapid crystallization rate.

3.2. Crystallinity

The crystallinities of annealed PLA and PLA/PPZn blends were investigated by XRD. Fig. 2a shows the XRD patterns of the PLA_{am} with various annealing times at $110 \text{ }^\circ\text{C}$. In addition to a sharp diffraction peak at 16.5° ($110/200$ lattice planes), two noticeable small peaks were also observed at 18.9° (203 lattice plane) and 22.3° (015 lattice plane) after 10 min of annealing. As shown in Table 2, the CrI of PLA showed 21.5% at 10 min, and then increased slightly to 24.2% at 60 min of annealing. These peaks are attributed

Table 1
Nonisothermal and isothermal crystallization of amorphous PLA and PLA/PPZn blends.

Sample code	PPZn (wt%)	Cooling ^a			Heating ^b			$t_{1/2}^c$ (min)
		T_{mc} (°C)	ΔH_{mc} (J/g)	X_{mc} (%)	T_{cc} (°C)	ΔH_{cc} (J/g)	X_{cc} (%)	
PLA _{am}	0	ND	ND	ND	114.2	50.2	54.0	28.1
N _{0.5}	0.5	123.4	54.4	58.7	ND	ND	ND	0.8
N ₁	1.0	124.1	54.2	58.8	ND	ND	ND	0.8
N ₃	3.0	126.5	56.8	63.0	ND	ND	ND	0.6
N ₅	5.0	127.9	59.5	67.3	ND	ND	ND	0.5

^a Nonisothermal melt crystallization at a 1st cooling rate of 10 °C/min.^b Nonisothermal cold crystallization at a 2nd heating rate of 20 °C/min.^c Isothermal crystallization half-time at 130 °C.**Fig. 2.** The XRD patterns of amorphous PLA with various annealing times at 110 °C (a) and of the PLA/PPZn blends with different PPZn concentrations (b).

to the diffraction of α form crystal planes for the crystallized PLA [33], and the intensity increased with increasing annealing time, which was likely caused by the development of ordered crystallites and the formation of crystalline structures throughout the annealing process [34].

On the other hand, the XRD patterns of the PLA with various amounts of PPZn are shown in Fig. 2b. Except for the diffraction peaks of crystallized PLA between 15 and 25°, two additional diffraction peaks are clearly observed for all the PLA/PPZn blends. The diffraction peaks at 6.1° and 12.3° are attributed to the diffraction from the (010) and (004/103) lattice planes of PPZn,

respectively [14], and the intensity of these peaks increased considerably with increasing PPZn concentration. In addition, as shown in Table 2, the CrI of PLA with 0.5 wt% PPZn increased by 17.6-fold compared to PLA_{am}. However, all the PLA/PPZn blends reached almost complete crystallization after compression molding, and there was no significant difference in crystallinity among them. This behavior is consistent with the nonisothermal and isothermal crystallization results described above. The rapid crystallization rate of the PLA/PPZn blends could be due to a nucleating mechanism that is caused by epitaxial nucleation. According to the literature [17,18,35], the c axis length of the PLA crystal ($c = 2.88$ nm) is twice the b axis length ($b = 1.445$ nm) of the PPZn crystal; thus, PLA crystals could undergo significant growth on the surface of the PPZn crystal.

3.3. Dynamic mechanical properties

The result obtained from XRD confirmed that the addition of PPZn in PLA matrix was sufficient to increase the crystallinity after compression molding. The effects of annealing and PPZn on the dynamic mechanical property or thermal resistance of the PLA blends are discussed further in this section. Fig. 3 shows the storage modulus (E') and loss tangent ($\tan \delta$) of the annealed PLA and PLA/PPZn blends as a function of temperature. A precipitous drop in E' of all samples can be expected near the T_g of the PLA (ca. 56 °C) [36]. However, for the annealed PLA, the E' increased with increasing annealing duration at temperatures above the T_g . As an example of E' at a level of 300 MPa, Fig. 3a shows that the correspondence temperature ranged from 65 to 67 °C for the PLA_{am}, A₂, and A₅. However, once the annealing duration reached 10 min, the temperature was increased significantly to 139.4 °C. This phenomenon can be explained by the increase in the crystalline region of a sample during the annealing process. In addition, for the PPZn-loaded PLA blends, all the temperatures were above 150 °C, and this value increased with increasing PPZn concentration. Accordingly, PLA/PPZn blends exhibited higher thermal resistance compared to the annealed PLA.

$\tan \delta$, a measure of material-related damping properties, is an indication of molecular motions in the materials, which contributes at the interface to damping or energy dissipation [37,38]. As illustrated in Fig. 3b, the intensity of the $\tan \delta$ peak decreased with increasing annealing duration. In addition, it can be clearly observed that the T_g ($\tan \delta$ peak) of the PLA shifts from the original 69.6 °C–75.6 °C after 60 min of annealing. In contrast, all the PLA/PPZn blends exhibited a greater decrease in the $\tan \delta$ intensity than the annealed PLA. The hypothesized explanation for this occurrence is that, in addition to the increase in the crystallinity, PPZn particles are considerably harder than the surrounding matrix, and they can increase the blend stiffness. However, the T_g of PLA/PPZn blends exhibits a slight shift to a lower temperature with increasing PPZn concentration. Theoretically, the T_g of a matrix should

Table 2
Glass transition temperature, crystallinity, and flexural properties of PLA annealed at different times and nucleated at different PPZn concentrations.

Sample code	Annealing (min)	PPZn (wt%)	T_g (°C) ^a	CrI (%) ^b	Density ^c (kg/m ³)	Flexural properties ^c	
						MOR (MPa)	MOE (GPa)
PLA _{am}	0	—	69.6	1.5	1209 ± 12 ^{A,X}	100.1 ± 9.2 ^{A,X}	3.58 ± 0.23 ^{A,B,C,Y}
A ₂	2	—	69.9	2.0	1181 ± 43 ^A	98.7 ± 3.2 ^{AB}	3.45 ± 0.12 ^C
A ₅	5	—	69.7	2.9	1201 ± 45 ^A	92.7 ± 5.7 ^B	3.48 ± 0.17 ^{BC}
A ₁₀	10	—	73.0	21.5	1196 ± 36 ^A	99.8 ± 2.0 ^{AB}	3.75 ± 0.06 ^{AB}
A ₁₅	15	—	73.8	22.8	1220 ± 02 ^A	94.4 ± 3.4 ^{AB}	3.80 ± 0.20 ^A
A ₃₀	30	—	74.3	23.6	1224 ± 06 ^A	95.9 ± 4.6 ^{AB}	3.89 ± 0.07 ^A
A ₆₀	60	—	75.6	24.2	1209 ± 29 ^A	93.2 ± 6.6 ^B	3.85 ± 0.15 ^A
N _{0.5}	—	0.5	69.7	26.4	1203 ± 25 ^X	83.1 ± 1.3 ^Y	4.23 ± 0.08 ^X
N ₁	—	1.0	69.4	28.4	1203 ± 43 ^X	79.7 ± 5.8 ^Y	4.34 ± 0.17 ^{X,Y}
N ₃	—	3.0	69.0	25.9	1203 ± 52 ^X	61.7 ± 3.2 ^Z	4.39 ± 0.21 ^X
N ₅	—	5.0	68.7	27.7	1224 ± 42 ^X	50.6 ± 4.9 ^Z	4.56 ± 0.19 ^X

^a Data from DMA.

^b Data from XRD.

^c Values are means ± SD ($n = 6$). Different letters within a column indicate significant differences at $P < 0.05$.

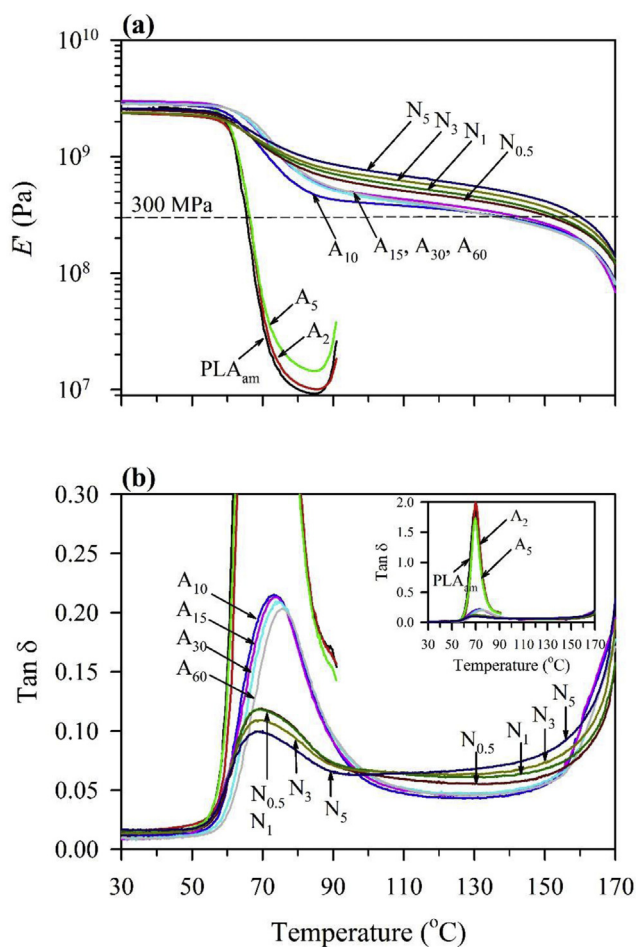


Fig. 3. Effects of annealing condition and PPZn concentration on the storage modulus (a) and $\tan \delta$ (b) of PLA and PLA/PPZn blends.

increase with increasing PPZn concentration because it induces smaller spherulite to increase crystallinity. One possible explanation for this observation is that the thermal degradation of the polymeric matrix could be induced during blending process, as reported by some studies [39–41]. In addition, Tanniru et al. [42] researched the increase in weak interaction between the filler and the matrix. In this study, GPC analysis was used to determine the changes in molecular weight during blending process of

specimens. As shown in Table 3, when 0.5 wt% PPZn was added into PLA matrix, the results reveal that the M_n and M_w of PLA/PPZn blend increased slightly by 7.5% (83.6 kg/mol) and 9.4% (123.5 kg/mol), respectively. Once the added PPZn is in excess of 0.5 wt%, the M_n and M_w values will significantly decrease with increasing PPZn concentration. Accordingly, the decrease in the molecular weight of PLA/PPZn blend was resulted from main-chain scission. This result provided further evidence of the thermal degradation of polymeric matrix during blending process of PPZn-loaded PLA blend, which leading to the T_g of PLA/PPZn blends is lower than that of the annealed PLA.

3.4. Flexural test

The static mechanical properties of the annealed PLA and PLA/PPZn blends were measured by the three-point bending test. As shown in Table 2, the MOR of all the annealed PLA exhibited no significant difference, whereas the MOE increased from 3.45 GPa at 2 min of annealing to 3.75 GPa at 10 min, and then it plateaued. For PLA/PPZn blends, the MOR decreased significantly by approximately 50% when adding 5 wt% PPZn in the PLA matrix. It was hypothesized that the probability of filler aggregation increased with increasing filler concentration to create localized regions of stress [17,43]. Conversely, the MOE increased by 18.2% to 4.23 GPa for 0.5 wt% PPZn-loaded PLA blends, and there were no significant differences between the MOE of the blends with various amounts of PPZn. Hence, it was determined that the incorporation of PPZn significantly improves the MOE of PLA.

3.5. Creep behavior

The effects of PPZn on the creep behavior of PLA blends were measured by DMA using the time–temperature superposition principle (TTSP). Fig. 4a shows the strong temperature dependence

Table 3

Number average molecular weight (M_n) and weight average molecular weight (M_w) of PLA/PPZn blends with different PPZn concentrations.

PPZn (wt%)	M_n (kg/mol)	M_w (kg/mol)
0	77.8 ± 0.3 ^B	112.9 ± 0.6 ^B
0.5	83.6 ± 1.3 ^A	123.5 ± 2.7 ^A
1.0	81.2 ± 1.7 ^A	118.8 ± 2.5 ^A
3.0	74.9 ± 0.7 ^B	112.2 ± 0.9 ^B
5.0	68.9 ± 0.8 ^C	101.9 ± 1.9 ^C

Values are means ± SD ($n = 3$). Different letters within a column indicate significant differences at $P < 0.05$.

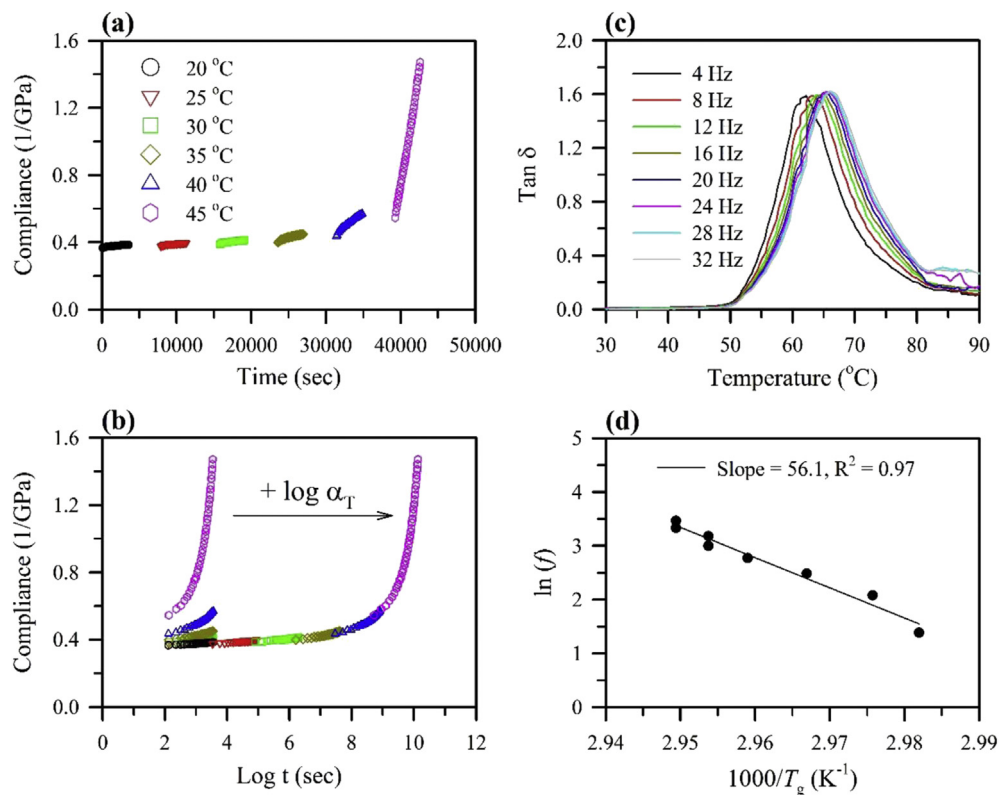


Fig. 4. (a) Effects of creep test temperature on creep compliance of amorphous PLA. (b) Unshifted and shifted creep compliance data of amorphous PLA using a reference temperature of 20 °C. (c) Tan δ curves for a range of frequencies at a heating rate of 1 °C/min. (d) Frequency in a log scale versus the inverse of T_g .

of the creep behavior for PLA_{am}. As expected, the creep compliance increased with increasing temperature, indicating that the reduction in stiffness of the entangled network of polymer chains results in the temperature-activated softening of the polymer matrix. Fig. 4b shows unshifted creep compliance data in a log time scale and shifted creep compliance data according to the reduced time using a shift factor (α_T) calculated from TTSP. Fig. 4c shows tan δ curves for a range of frequencies at a heating rate of 1 °C/min. The T_g at different frequencies was determined from the peak of the tan δ curves and the E_a is calculated from the slope of the plot of $\ln(f)$ versus $1/T_g$ as shown in Fig. 4d. According to this calculation, the E_a values of PLA_{am}, annealed PLA, and PLA blends with various PPZn concentrations were in the range of 455.7–471.3 kJ/mol (Table 4). Consequently, as shown in Fig. 5a, the creep compliance master curves of the various specimens generated using shift factors are estimated from a constant activation energy assumption. Fig. 5b shows the creep master curves which were modeled with the Findley power law in a normal time scale; the instantaneous elastic

compliances (S_0) and the predicted reductions in the modulus levels of all specimens over 1–60 year periods are tabulated in Table 4. The $S(t)$ of PLA_{am} showed 0.43, 0.54, 0.60, and 0.68 GPa⁻¹ at 1, 15, 30, and 60 years, respectively. Once the PPZn concentration increased to 0.5 wt %, the predicted compliance declined to 0.43, 0.48, 0.50, and 0.52 GPa⁻¹ at 1, 15, 30, and 60 years, respectively. Furthermore, in order to estimate the creep resistance of a sample under long-term conditions, the reduction in modulus was calculated by the following equation: modulus reduction (%) = $[1 - S_0/S(t)] \times 100$ [31]. The modulus of PLA_{am} would reduce by 42.9% at 60 years. However, the reduction in modulus of the annealed PLA (A_{60}) was only 22.3% at 60 years. This result revealed that the generation of the crystal region in PLA matrix could improve the creep resistance. Similar results were reported that the degree of crystallinity significantly affects the creep behavior in semicrystalline polymers [44,45]. For PPZn-loaded PLA blends, the modulus of all specimens would reduce in a concentration-dependent manner. This result indicated that the increase in PPZn concentration in PLA matrix

Table 4

Activation energy and the predicted reductions in modulus of amorphous PLA, annealed PLA, and PLA/PPZn blends using a reference temperature of 20 °C.

Sample code	S_0 (GPa ⁻¹)	a	b	$S(t)$ (GPa ⁻¹)				Reduction in modulus (%)				Activation energy (kJ/mol)
				Time (years)				Time (years)				
				1	15	30	60	1	15	30	60	
PLA _{am}	0.39	1.18×10^{-5}	0.47	0.43	0.54	0.60	0.68	9.6	28.0	35.1	42.9	466.4
N _{0.5}	0.35	2.88×10^{-3}	0.19	0.43	0.48	0.50	0.52	17.7	26.8	29.4	32.2	461.8
N ₁	0.36	1.03×10^{-3}	0.21	0.41	0.44	0.45	0.47	10.3	17.1	19.3	21.7	471.3
N ₃	0.41	1.85×10^{-5}	0.41	0.43	0.47	0.50	0.53	5.1	14.3	18.1	22.7	455.7
N ₅	0.40	1.78×10^{-6}	0.51	0.41	0.45	0.47	0.50	3.0	11.1	15.1	20.2	458.7
A ₆₀	0.37	7.69×10^{-5}	0.34	0.39	0.43	0.45	0.47	6.6	15.3	18.3	22.3	456.5

$S(t) = S_0 + at^b$, where $S(t)$ is the time-dependent compliance, S_0 is the instantaneous elastic compliance, a and b are constant numbers.

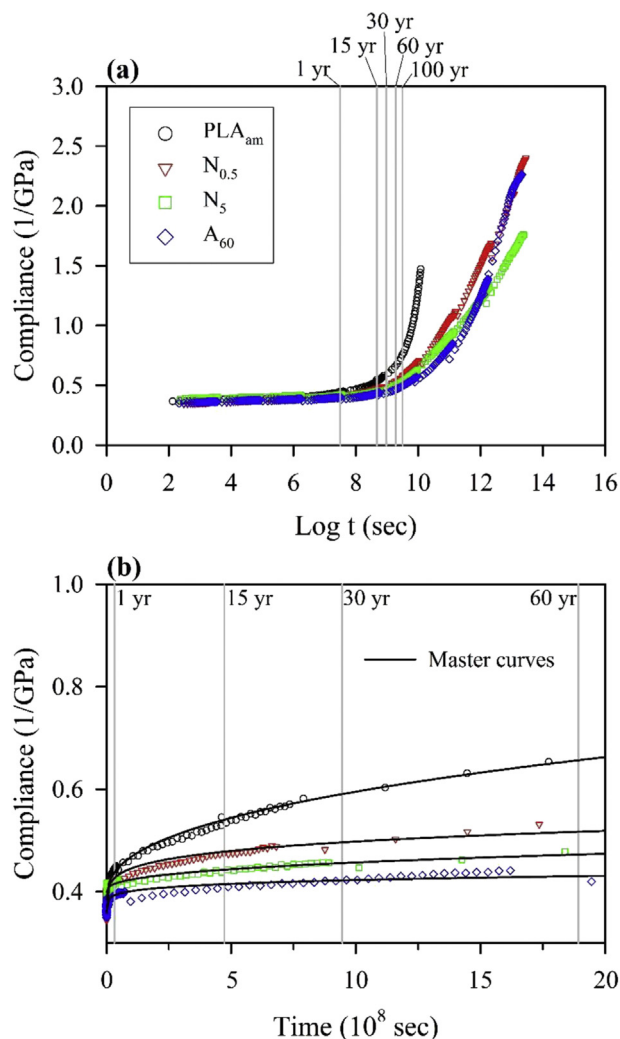


Fig. 5. Creep master curves of amorphous PLA, annealed PLA, and PLA/PPZn blends in a log time scale (a) and in a normal time scale (b) using a reference temperature of 20 °C.

significantly improves creep resistance. Additionally, the modulus reduction of all the PLA/PPZn blends was still less than 33% over the 60-year period. Comparison of the modulus retentions between PPZn-loaded PLA blends and annealed PLA did not indicate a noticeable difference. The result is consistent with that of Raff et al. [46] who described that the flexural creep was unchanged although the nucleation density increased. However, according to the increase rate of the compliance (b value of the Findley power law), the 0.5–1.0 wt% PPZn-loaded PLA blends showed the smallest b value (ca. 0.2) among all the specimens. Taken together, these results verified that a minimal PPZn concentration as a nucleating agent in PLA matrix would significantly increase the creep resistance.

4. Conclusions

The static and dynamic mechanical properties and creep resistance of PLA and PLA-based blends are greatly influenced by their crystallization behavior. Zinc phenylphosphonate (PPZn) is as an excellent nucleating agent for PLA. The addition of PPZn into PLA could significantly accelerate the crystallization of PLA in a concentration-dependent manner. Even with the addition of 0.5 wt % PPZn, the isothermal crystallization half-time ($t_{1/2}$) of PLA/PPZn

blend was less than 1 min. Conversely, the $t_{1/2}$ value of PLA_{am} was 28.1 min. This result implies that the addition of PPZn into PLA matrix is applicable for industrial mold processing due to its rapid crystallization rate. Although the modulus of rupture (MOR) of PLA/PPZn blends decreased with increasing PPZn concentration, the modulus of elasticity (MOE) of all the blends were improved when adding PPZn in PLA. However, the thermal resistance of all PLA with PPZn particles was higher than that of the annealed PLA over the glass transition temperature range. In addition, the predicted modulus reduction of PLA_{am} was reduced by approximately 43% over the 60-year period, whereas the reduction in modulus of PLA blend with 1 wt% PPZn was still less than 22%. A similar result was observed for the PLA annealed at 110 °C for 60 min. Accordingly, the crystallization rate, thermal resistance, and creep property of PLA could be considerably improved by the addition of PPZn to only a few weight percent.

Acknowledgments

This work was financially supported by a research grant from the Ministry of Science and Technology, Taiwan (MOST 102-2628-B-005-006-MY3).

References

- [1] S.S. Im, Y.H. Kim, J.S. Yoon, I.J. Chin, *Bio-based Polymers: Recent Progress*, Wiley-VCH, Germany, 2005.
- [2] H. Tsuji, Y. Ikada, *Properties and morphologies of poly(L-lactide): 1. Annealing condition effects on properties and morphologies of poly(L-lactide)*, *Polymer* 36 (14) (1995) 2709–2716.
- [3] A.M. Harris, E.C. Lee, *Improving mechanical performance of injection molded PLA by controlling crystallinity*, *J. Appl. Polym. Sci.* 107 (4) (2008) 2246–2255.
- [4] S.D. Park, M. Todo, K. Arakawa, *Effect of isothermal crystallization on fracture toughness and crack growth behavior of poly(lactic acid)*, *J. Mater. Sci.* 40 (4) (2005) 1055–1058.
- [5] M. Day, A. Victoria, X. Liao, *A DSC study of the crystallization behaviour of polylactic acid and its nanocomposites*, *J. Therm. Anal. Calorim.* 86 (2006) 623–629.
- [6] H. Tsuji, H. Takai, S.K. Saha, *Isothermal and non-isothermal crystallization behavior of poly(L-lactic acid): Effects of stereocomplex as nucleating agent*, *Polymer* 47 (11) (2006) 3826–3837.
- [7] A. Pei, Q. Zhou, L.A. Berglund, *Functionalized cellulose nanocrystals as bio-based nucleation agents in poly(L-lactide) (PLLA): Crystallization and mechanical property effects*, *Compos. Sci. Technol.* 70 (5) (2010) 815–821.
- [8] F. De Santis, R. Pantani, G. Titomanlio, *Nucleation and crystallization kinetics of poly(lactic acid)*, *Thermochim. Acta* 522 (1–2) (2011) 128–134.
- [9] N. Kawamoto, A. Sakai, T. Horikoshi, T. Urushihara, E. Tobita, *Nucleating agent for poly(L-lactide): An optimization of chemical structure of hydrazide compound for advanced nucleation ability*, *J. Appl. Polym. Sci.* 103 (1) (2007) 198–203.
- [10] H. Li, M.A. Huneault, *Effect of nucleation and plasticization on the crystallization of poly(lactic acid)*, *Polymer* 48 (23) (2007) 6855–6866.
- [11] T. Ke, X. Sun, *Melting behavior and crystallization kinetics of starch and poly(lactic acid) composites*, *J. Appl. Polym. Sci.* 89 (5) (2003) 1203–1210.
- [12] J.Y. Nam, S.S. Ray, M. Okamoto, *Crystallization behavior and morphology of biodegradable polylactide/layered silicate nanocomposite*, *Macromolecules* 36 (19) (2003) 7126–7131.
- [13] N. Ogata, G. Jimenez, H. Kawai, T. Ogihara, *Structure and thermal/mechanical properties of poly(L-lactide)-clay blend*, *J. Polym. Sci. Pol. Phys.* 35 (2) (1997) 389–396.
- [14] S.S. Ray, K. Yamada, M. Okamoto, Y. Fujimoto, A. Ogami, K. Ueda, *New polylactide/layered silicate nanocomposites. 5. Designing of materials with desired properties*, *Polymer* 44 (21) (2003) 6633–6646.
- [15] Y. Xu, L. Wu, *Synthesis of organic bisurea compounds and their roles as crystallization nucleating agents of poly(L-lactic acid)*, *Eur. Polym. J.* 49 (4) (2013) 865–872.
- [16] S.M. Lai, S.H. Wu, G.G. Lin, T.M. Don, *Unusual mechanical properties of melt-blended poly(lactic acid) (PLA)/clay nanocomposites*, *Eur. Polym. J.* 52 (2014) 193–206.
- [17] P. Pan, Z. Liang, A. Cao, Y. Inoue, *Layered metal phosphonate reinforced poly(L-lactide) composites with a highly enhanced crystallization rate*, *ACS Appl. Mater. Inter.* 1 (2) (2009) 402–411.
- [18] G. Cao, H. Lee, V.M. Lynch, T.E. Mallouk, *Synthesis and structural characterization of a homologous series of divalent-metal phosphonates, $M^{II}(\text{O}_3\text{PR})\cdot\text{H}_2\text{O}$ and $M^{II}(\text{HO}_2\text{PR})_2$* , *Inorg. Chem.* 27 (16) (1988) 2781–2785.
- [19] S. Wang, C. Han, J. Bian, L. Han, X. Wang, L. Dong, *Morphology, crystallization and enzymatic hydrolysis of poly(L-lactide) nucleated using layered metal*

- phosphonates, *Polym. Int.* 60 (2) (2011) 284–285.
- [20] Y. Miyano, M. Kanemitsu, T. Kunio, H. Kuhn, Role of matrix resin on fracture strengths of unidirectional CFRP, *J. Compos Mater* 20 (6) (1986) 520–538.
- [21] B. Abdel-Magid, R. Lopez-Anido, G. Smith, S. Trofka, Flexure creep properties of E-glass reinforced polymers, *Compos Struct.* 62 (3–4) (2003) 247–253.
- [22] X. Wang, J. Shi, J. Liu, L. Yang, Z. Wu, Creep behavior of basalt fiber reinforced polymer tendons for prestressing application, *Mater. Des.* 59 (2014) 558–564.
- [23] G.H. Doh, I.A. Kang, S.Y. Lee, Y.T. Kong, C.S. Jeong, B.S. Lim, Mechanical properties and creep behavior of liquefied wood polymer composites (LWPC), *Compos Struct.* 68 (2) (2005) 225–233.
- [24] L. Suryanegara, A.N. Nakagaito, H. Yano, Thermo-mechanical properties of microfibrillated cellulose-reinforced partially crystallized PLA composites, *Cellulose* 17 (4) (2010) 771–778.
- [25] L. Rozite, J. Varna, R. Joffe, A. Pupurs, Nonlinear behavior of PLA and lignin-based flax composites subjected to tensile loading, *J. Thermoplast. Compos Mater* 26 (4) (2013) 476–496.
- [26] E. Kontou, G. Spathis, P. Georgiopoulos, Modeling of nonlinear viscoelasticity-viscoplasticity of bio-based polymer composites, *Polym. Degrad. Stabil.* 110 (2014) 203–207.
- [27] M.S. Islam, K.L. Pickering, N.J. Foreman, Influence of accelerated ageing on the physico-mechanical properties of alkali-treated industrial hemp fibre reinforced poly(lactic acid) (PLA) composites, *Polym. Degrad. Stabil.* 95 (1) (2010) 59–65.
- [28] Y. Srithep, P. Nealey, L.S. Turng, Effects of annealing time and temperature on the crystallinity and heat resistance behavior of injection-molded poly(lactic acid), *Polym. Eng. Sci.* 53 (2013) 580–588.
- [29] Y. Xu, Q. Wu, Y. Lei, F. Yao, Creep behavior of bagasse fiber reinforced polymer composites, *Bioresour. Technol.* 101 (9) (2010) 3280–3286.
- [30] A.J. Nuñez, N.E. Marcovich, M.I. Aranguren, Analysis of the creep behavior of polypropylene-woodflour composites, *Polym. Eng. Sci.* 44 (8) (2004) 1594–1603.
- [31] W.K. Goertzen, M.R. Kessler, Creep behavior of carbon fiber/epoxy matrix composites, *Mater. Sci. Eng. A Struct Mater Prop. Microstruct. Process* 421 (1–2) (2006) 217–225.
- [32] W.N. Findley, J.S. Lai, K. Onaran, *Creep and Relaxation of Nonlinear Viscoelastic Materials—with an Introduction to Linear Viscoelasticity*, Dover Publications, New York, 1976.
- [33] K. Das, D. Ray, I. Banerjee, N.R. Bandyopadhyay, S. Sengupta, A.K. Mohanty, M. Misra, Crystalline morphology of PLA/clay nanocomposite films and its correlation with other properties, *J. Appl. Polym. Sci.* 118 (1) (2010) 143–151.
- [34] P.M. Chou, M. Mariatti, A. Zulkifli, M. Todo, Changes in the crystallinity and mechanical properties of poly(L-lactic acid)/poly(butylene succinate-co-L-lactate) blend with annealing process, *Polym. Bull.* 67 (5) (2011) 815–830.
- [35] W. Hoogsteen, A.R. Postema, A.J. Pennings, G. Ten Brinke, P. Zugenmaier, Crystal structure conformation and morphology of solution-spun poly(L-lactide) fibers, *Macromolecules* 23 (2) (1990) 634–642.
- [36] B.H. Lee, H.S. Kim, S. Lee, H.J. Kim, J.R. Dorgan, Bio-composites of kenaf fibers in polylactide: Role of improved interfacial adhesion in the carding process, *Compos Sci. Technol.* 69 (15–16) (2009) 2573–2579.
- [37] C.K. Hong, N. Kim, S.L. Kang, C. Nah, Y.S. Lee, B.H. Cho, J.H. Ahn, Mechanical properties of maleic anhydride treated jute fibre/polypropylene composites, *Plast. Rubber Compos* 37 (7) (2008) 325–330.
- [38] Y.L. Chen, C.Y. Lin, T.L. Wu, M.J. Chung, T.Y. Chen, T.H. Yang, H.C. Chen, J.H. Wu, Evaluation and application of the invasive weed *Mikania micrantha* as an alternative reinforcement in recycled high density polyethylene, *Bioresources* 7 (2) (2012) 2403–2417.
- [39] P. Pötschke, A.R. Bhattacharyya, A. Janke, H. Goering, Melt mixing of polycarbonate/multi-wall carbon nanotube composites, *Compos. Interface* 10 (4–5) (2003) 389–404.
- [40] R. Andrews, D. Jacques, M. Minot, T. Rantell, Fabrication of carbon multiwall nanotube/polymer composites by shear mixing, *Macromol. Mater Eng.* 287 (2002) 395–403.
- [41] B.J. Ash, R.W. Siegel, L.S. Schadler, Glass-transition temperature behavior of alumina/PMMA nanocomposites, *J. Polym. Sci. Part B Polym. Phys.* 42 (23) (2004) 4371–4383.
- [42] M. Tanniru, Q. Yuan, R.D.K. Misra, On significant retention of impact strength in clay-reinforced high-density polyethylene (HDPE) nanocomposites, *Polymer* 47 (6) (2006) 2133–2146.
- [43] S. Jain, M. Misra, A.K. Mohanty, A.K. Ghosh, Thermal, mechanical and rheological behavior of poly(lactide acid)/talc composites, *J. Polym. Environ.* 20 (4) (2012) 1027–1037.
- [44] B.E. Read, P.E. Tomlins, Creep and physical aging of injection molding, fiber reinforced polypropylene, *Polym. Eng. Sci.* 37 (9) (1997) 1572–1581.
- [45] B.A. Acha, M.M. Reboredo, N.E. Marcovich, Creep and dynamic mechanical behavior of PP–jute composites: effect of the interfacial adhesion, *Compos Part A Appl S* 38 (6) (2007) 1507–1516.
- [46] R.A.V. Raff, A.S. Ahmad, Dependence of properties on spherulite size in crystalline polymers, *Northwest Sci.* 44 (1970) 184–205.